LA-UR- 11-04661

Approved for public release; distribution is unlimited.

Title:	DFT Calculations for the Uranium EOS
Author(s):	Carl Greeff, Scott Crockett, Sven Rudin, John Wills
Intended for:	APS SCCM 2011

Los Alamos
NATIONAL LABORATORY
EST. 1943

Form 836 (7/06)

DFT Calculations for the Uranium EOS

C. W. Greeff, S. D. Crockett, S. P. Rudin, and J. M. Wills

T-1, MS-B221, LANL, Los Alamos, NM 87545

Abstract. We present results of density functional theory calculations on the Uranium equation of state. We examine the influence of approximations for the exchange-correlation functional. By comparing DFT calculations with an empirical EOS we find that the PBE functional gives good results for the EOS of the α phase. Calculations on the γ phase, which is bcc, show it to exhibit elastic and phonon instabilities. The electron temperature significantly influences the effective nuclear potential.
Keywords: Uranium, Equation of State, Density Functional Theory
PACS: 64.30.-t,64.70.D-

INTRODUCTION

It is challenging to obtain accurate equations of state (EOS) for actinides. Standard model approximations used in empirical EOS [1], such as the independence of electronic and nuclear excitations, may be inaccurate due to the narrow $5f$ bands. In addition, predictions of EOS parameters from first principles are more challenging to theory than for simple metals or transition metals.

Here we focus on the equation of state and phase diagram of uranium metal. For the uranium, the $5f$ electrons are itinerant at ambient pressure. Under pressure, the itinerant nature is expected to be enhanced. Thus, uranium under compression is not expected to exhibit strong electron correlation effects, and may be amenable to standard density functional calculations.

The ambient temperature and pressure α structure of uranium is orthorhombic, with four atoms per (conventional) unit cell [2, 3]. On increasing temperature at ambient pressure, it undergoes two solid-solid phase transitions to the β and γ phases. The γ phase has a bcc crystal structure, and persists as the high temperature phase to pressures of at least 60 GPa [4]. Since the β phase only exists in a very small wedge of the P,T plane, we will focus exclusively on the α and γ phases here.

DFT CALCULATIONS

The DFT calculations presented here use the plane-wave code *abinit* [5]. Most of the calculations use the projector augmented wave (PAW) method [6], while some use norm-conserving (NC) pseudopotential [7]. The calculations use a planewave cutoff of 30 E_H (E_H denotes the Hartree energy unit, E_H = 27.2114 eV) for PAW and 40 E_H for the NC pseudopotential. The k-point meshes were $16 \times 16 \times 8$ for the α structure and 16^3 for bcc, with a Gaussian smearing parameter of 0.01 E_H.

The PAW and norm-conserving pseudopotentials were generated by us using the code *atompaw* [8] and J. L. Martins' *atom* code [7], respectively. The semi-core $6s$ and $6p$ electrons are treated as active, while the $5d$ electrons are included in the core, giving 14 electrons that are explicitly treated. The PAW employs two projectors per angular momentum channel, up to f-type, while the NC pseudopotential uses one per channel. Scalar relativistic effects are included in the generation of the PAW and pseudopotential.

α PHASE

Table 1 gives the crystal structure parameters of α-U calculated with the PAW method using various

TABLE 1. Calculated structural properties of α-U. All lengths in units of a_0. Approximate exchange correlation functionals are PBE [10], WC [11], and LDA [12]. Experimental measurement is at 50 K, above the charge density wave transitions [2].

method	functional	a	b	c	y	V
PAW	PBE	5.32	11.03	9.30	0.099	136.4
PAW	LDA	5.16	10.81	9.12	0.098	127.2
PAW	WC	5.24	10.91	9.22	0.098	131.6
NC	PBE	5.41	10.66	9.46	0.106	136.3
FPLMTO [9]	PBE	5.35	10.95	9.37	0.102	137.2
Expt. [2]		5.36	11.09	9.33	0.102	138.6

exchange correlation functionals, along with a full-potential LMTO calculation [9] and experimental data [2]. The present PAW calculation with the PBE [10] functional is in good agreement with experiment and with the corresponding full-potential calculation. The WC [11] and LDA [12] give successively smaller volumes, as is typical [13]. It is usually found for solids that the PBE volume is too large [13], but for U, the PBE volume is somewhat too small, with the other functionals being worse. Our NC pseudopotential gives nearly the same volume as the PAW, but the individual lattice parameters are rather different, with b smaller by 3%. It was found that the NC lattice parameters varied substantially depending on the occupations of the atomic state used to generate the pseudopotential.

Figure 1 shows the ratios of lattice parameters as a function of compression, as calculated with various functionals, along with diffraction data from diamond anvil cell experiments by LeBihan *et al.* [9] There is very little difference among the functionals, all of which capture the absolute lattice parameters and anisotropy of compression quite well, when plotted as a function of the volume.

It is in the relation of volume to pressure that the functionals are distinct. This is shown in figure 2, which shows the static lattice pressure from the different functionals, along with the empirically derived result. Our empirical EOS uses ambient pressure thermodynamic and elastic data, together with static high-pressure data [9] as input. We see that the PBE calculation agrees well with the empirical result. The difference in volume is 1.5% at $P = 0$, and decreases at higher pressures. The WC functional often gives superior results to PBE [13], but that is not the case for U.

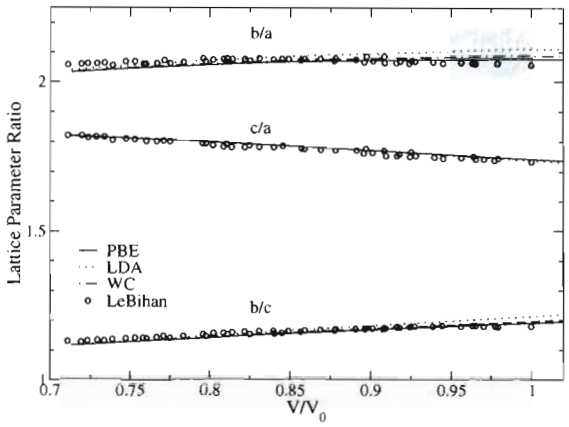

FIGURE 1. Ratios of lattice parameters of α-U under compression. DFT calculations use PAW method with various exchange correlation functionals. Diffraction data are from LeBihan *et al.* [9].

The phonon frequencies are important contributors to the EOS. Bouchet [14] has done DFT calculations of the α-U phonon frequencies over a range of densities. From the given self-force constants we have calculated the second moment of the phonon frequencies at ambient pressure, and obtain $\theta_2 =$ 168 K, while the effective Debye temperature in our empirical EOS is 173 K. The empirical value is derived from experimental data on the specific heat and entropy. Thus we find good consistency between the thermodynamic data and the DFT phonon dispersions, which in turn agree well with neutron scattering data.

Generally, we have found that for α-U, there is good correspondence between thermodynamic models and the underlying physical properties, and that DFT, with the PBE functional, gives good predic-

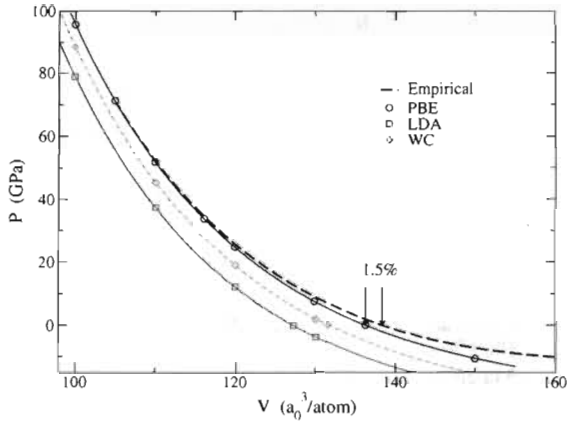

FIGURE 2. Static lattice pressure of α-U. DFT calculations with three different functionals are compared with an empirical result.

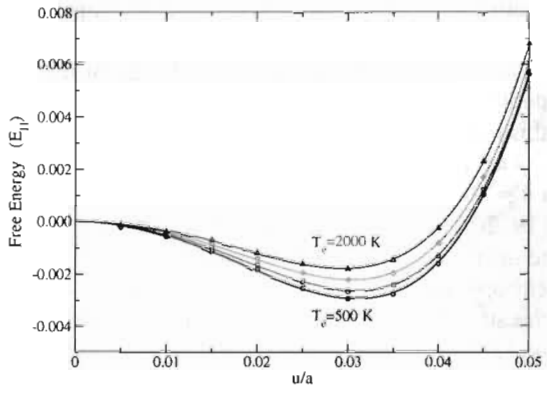

FIGURE 3. Effect of electron temperature on the potential for atomic displacement. The atoms at the center and corner of the conventional bcc cell are moved toward each other.

tions for these properties. One exception is electronic specific heat. Our PBE calculations give an electronic specific heat coefficient of 5.5 J/mol K^2, whereas the measured value is 9.1 J/mol K^2 [15]. Chantis *et al.* [16] used the GW method to estimate that many-body effects lead to an enhancement by a factor of 1.22. The remaining difference may plausibly be due to electron-phonon interactions. This suggests that there are significant errors in standard DFT for this quantity. This type of error is small for many EOS applications, but may be significant for the phase diagram, because the electronic entropy is exceptionally large for U.

γ PHASE

The γ phase has the bcc structure. It is stable above 1050 K at ambient pressure, and persists as the high-temperature phase to at least 60 GPa [4]. It is known that in PBE static lattice calculations, the bcc structure is unstable with respect to tetragonal distortions [3]. We confirm this instability, and find that it persists for volumes from 140 through 110 a_0^3/atom, corresponding to a cold pressure of 50 GPa. For all volumes in this range, both the bcc and fcc structures are local maxima of the energy. The minimum energy structure along the Bain path is bct with $c/a = 0.8$. The bct structure is lower in energy than bcc by $4 - 5 \times 10^{-3} E_H$ over this range.

We have also examined the stability of the bcc structure with respect to displacement of the atoms at the corner and in the center of conventional unit cell towards one another. We find that bcc is also a local maximum with respect to this motion, meaning that the bcc structure is unstable with respect to a phonon at the N-point in the harmonic approximation.

These types of instability are not unheard of for high temperature bcc structures. For instance, the metals in the Ti column all exhibit instabilities in the harmonic approximation, as calculated by DFT. The current understanding is that DFT is correct, and strong anharmonicity must be accounted for [17] in order to describe these high-temperature phases.

Aside from anharmonicity, another effect that may be significant in U is coupling of electronic excitation and nuclear motion. To investigate the importance of this effect, we note that, for classical nuclear motion, the effective potential energy surface is the electronic *free energy*, which replaces the ground state energy at finite temperature [18]. In the calculations the free energy is approximated by including $-TS_{\mathrm{el}} = T\sum_i [f_i \ln f_i + (1-f_i)\ln(1-f_i)]$ self-consistently in the energy functional, where f_i is the Fermi occupation factor of state i.

Figure 3 shows the effect of varying the electron temperature on the effective potential for the unstable H-point phonon displacement. The curves are shifted to line up at zero displacement to emphasize the coupling of electron temperature to the shape of the ef-

fective nuclear potential. The range of temperatures extends somewhat above melting at this volume. It is seen that there is a significant change of the well depth (a useful relation is $10^{-3}E_H = k_B \times 316$ K), but this is not sufficient to stabilize the mode.

Our empirical EOS is multi-phase, and incorporates the γ phase thermodynamically consistently [19, 20], matching the experimental phase transition temperature, and thermodynamic data, such as the entropy and specific heat. The empirical EOS puts the static lattice energy of the γ phase above the α by $1.5 \times 10^{-3}E_H$, while our DFT calculations give an energy difference of $9.3 \times 10^{-3}E_H$. The empirical EOS uses a Debye model for the nuclear motion, so that its cold energy is an extrapolation to $T = 0$ from high tempertures using a nuclear specific heat of $3k_B$ per atom. It is possible that strong anharmonicity renders this extrapolation inaccurate. This should be considered, along with the possibility that the DFT energy difference is inaccurate.

CONCLUSIONS

We have done DFT calculations and constructed an empirical multi-phase equation of state for the α and γ phases of Uranium. Comparison between these and other calculations and data indicate that DFT with the PBE exchange-correlation functional describes most EOS properties of α-U accurately. The one exception is that the electronic density of states appears to be underestimated. DFT calculations on the γ phase show elastic and phonon instabilities in the static lattice and harmonic approximations, respectively. We also find that the DFT energy difference between the α and γ structures is significantly larger than our empirical EOS indicates.

At this point it is unclear whether DFT is consistent with the experimental facts concerning the phase transition temperature and thermodynamics of γ-U. It is clear that simplifications, such as the harmonic approximation and decoupling of nuclear motion and electronic excitation are not valid. Further progress on first-principles understanding of γ-U will require confronting strong anharmonicity as well as electron-nuclear coupling.

REFERENCES

1. R. M. More, K. H. Warren, D. A. Young, and G. B. Zimmerman, Phys. Fluids **31**, 3059 (1988).
2. C. S. Barrett, M. H. Mueller, and R. L. Hitterman, Phys. Rev. **129**, 625 (1963).
3. P. Söderlind, Advances in Physics, **47** 959 (1998).
4. C.-S. Yoo, H. Cynn, and P. Söderlind, Phys. Rev. B **57** (1998).
5. X. Gonze, J.-M. Beuken, R. Caracas, F. Detraux, M. Fuchs, G.-M. Rignanese, L. Sindic, M. Verstraete, G. Zerah, F. Jollet, M. Torrent, A. Roy, M. Mikami, Ph. Ghosez, J.-Y. Raty, D.C. Allan, Computational Materials Science **25**, 478-492 (2002).
6. P. E. Blöchl, Phys. Rev. B **50**, 17953 (1994).
7. N. Troullier and J. L. Martins Phys. Rev. B **43**, 1993 (1991).
8. N. A. W. Holzwarth, A. R. Tackett, and G. E. Matthews, Comput. Phys. Commun. **135**, 329 (2001); M. Torrent and N. A. W. Holzwarth, *A User's Guide for* atompaw *Code* August 27, 2007.
9. T. LeBihan, S. Heathman, M. Idiri, G. H. Lander, J. M. Wills, A. C. Lawson, and A. Lindbaum, Phys. Rev. B **67**, 134102 (2003).
10. J. P. Perdew, S. Burke, and M. Ernzerhof, Phys. Rev. Lett. **77**, 3865 (1996).
11. Z. G. Wu and R. E. Cohen, Phys. Rev. B **73**, 235116 (2006).
12. J. P. Perdew and Y. Wang, Phys. Rev. B **45**, 13244 (1992).
13. P. Haas, F. Tran, and P. Blaha, Phys. Rev. B **79**, 085104 (2009).
14. J. Bouchet, Phys. Rev. B **77**, 024113 (2008).
15. J. C. Lashley, B. E. Lang, J. Boerio-Goates, V. G. Woodfield, G. M. Schmiedeshoff, E. C. Gay, C. C. McPheeters, D. J. Thoma, W. L. Hults, J. C. Cooley R. J. Hanrahan, and J. L. Smith, Phys. Rev. B **63**, 224510 (2001).
16. A. N. Chantis, R. C. Albers, M. D. Jones, M. van Schilfgaarde, and T. Kotani, Phys. Rev. B **78**, 081101 (2008).
17. P. Souvatzis, O. Eriksson, M. I. Katsnelson, and S. P. Rudin, Phys. Rev. Lett. **100**, 95901 (2008).
18. R. W. Zwanzig, Phys. Rev. **106** 13 (1957).
19. E. D. Chisolm, et al., Los Alamos National Laboratory Report No. LA-UR-05-9413 (2005).
20. S. D. Crockett and C. W. Greeff, *AIP SCCM proceedings* **1195** 1191-1194 (2009).